

# Non-Hermitian three-dimensional two-band Hopf insulator

Yan He<sup>1</sup> and Chih-Chun Chien<sup>2</sup>

<sup>1</sup>*College of Physics, Sichuan University, Chengdu, Sichuan 610064, China*<sup>\*</sup>

<sup>2</sup>*School of Natural Sciences, University of California, Merced, CA 95343, USA.*<sup>†</sup>

The Hopf insulator is a three-dimensional topological insulator outside the standard classification of topological insulators. Here we consider a non-Hermitian generalization of the Hopf insulator with a generalized expression of the Hopf index. The isolated gapless points of the Hermitian model are broadened into finite regimes in the non-Hermitian model. However, the modulus of the Hopf index remains quantized in the gapped regions. While the gapless regimes estimated from the system with periodic- and open- boundary conditions agree well, the energy spectrum of the non-Hermitian Hopf model with open boundary condition shows localized states crossing the energy gap. Near the zero-energy plane, Fermi rings can be observed whenever the Hopf index is quantized at nonzero values. Moreover, we found a bulk-boundary correspondence between the modulus of the Hopf index and the number of Fermi rings.

## I. INTRODUCTION

The applications of topological concepts to condensed matter systems have brought us new paradigms for classifying materials<sup>1–3</sup>. While the conventional quantum mechanics deals with Hermitian systems, there have been studies on non-Hermitian systems with topological properties<sup>4–9</sup>. The energy spectra and wavefunctions of non-Hermitian systems can exhibit interesting behavior due to the possible appearance of complex numbers. The bulk-boundary correspondence relating the topological invariant of the bulk and the localized edge state at the boundary has been demonstrated in Hermitian topological systems<sup>1–3</sup>, but more careful analyses may be needed for non-Hermitian systems<sup>4,10–13</sup>. Using many-body approach, the observation and interpretation of non-Hermitian systems may differ<sup>14</sup>. Moreover, the influence of non-Hermitian systems on quantum dynamics has been analyzed<sup>15,16</sup>. While the Hermitian topological insulators may be classified according to their symmetries<sup>3</sup>, there have been different schemes for classifying non-Hermitian topological systems<sup>17–21</sup>. In addition to electronic materials, non-Hermitian systems may be relevant to optical<sup>22</sup>, acoustic<sup>23</sup>, mechanical<sup>24</sup>, or cold-atom<sup>25</sup> systems.

The Hermitian Hopf insulator is a two-band topological insulator (TI) in 3D, which is simpler than the four-band model of the AII-class TI. The ten-fold way classification of Hermitian gapped topological models is based on the stable homotopy groups<sup>3</sup>. In contrast, the existence of the Hopf insulator is due to the low dimensional homotopy of the Hopf mapping<sup>26</sup> from the three-sphere  $S^3$  to the two-sphere  $S^2$ . Therefore, the Hermitian Hopf insulator does not fit into the periodic table of topological insulators. The Hopf insulator with a unit Hopf index was introduced in Ref.<sup>27</sup>. Later, it was generalized to models with an arbitrary Hopf index<sup>28</sup>. It has been found that the number of edge states of the Hopf insulator with a higher Hopf index is usually larger than the corresponding Hopf index<sup>28</sup>, complicating the bulk-boundary correspondence. In this paper, we will only

consider the model constructed by the mapping with a unit Hopf index. Since the target space of the Hopf mapping is a 2D sphere, the Hopf insulator must be a two-band model. It becomes topologically trivial when more bands are added into the model. However, the Hopf insulators were recently generalized to models with multiple bands in Ref.<sup>29</sup>. The Hermitian Hopf insulator has been analyzed by quantum simulators<sup>30,31</sup>, and there may be other promising platforms for studying it<sup>32</sup>.

Here we investigate a non-Hermitian generalization of the Hopf insulator. Due to the non-Hermitian Hamiltonian, the energy spectrum may become complex. A generalization of the Hopf index for the non-Hermitian model is presented. In general, the Hopf index is complex, but its modulus exhibits quantization in the regimes similar to where the Hermitian Hopf insulator shows a quantized Hopf index. Therefore, we may still use the Hopf index to distinguish topologically distinct regimes. However, due to the non-Hermitian Hamiltonian, the gap-closing regions in the energy spectrum are broadened while the Hopf index drops towards zero in those regions. This is in contrast to the Hermitian case, where the gap only closes at isolated points with the Hopf index being undefined at those points.

By analyzing the energy spectrum of the non-Hermitian Hopf model with open boundary condition along one spatial direction, we found that the gapless regimes agree with those estimated from the same system with periodic boundary condition. Moreover, there are Fermi rings at zero energy indicating topological states crossing the band gap. A bulk-boundary correspondence relating the modulus of the generalized Hopf index and the number of Fermi rings was found in the non-Hermitian model. This is in contrast to some lower-dimensional models, where the bulk-boundary correspondence needs special treatments<sup>33,34</sup>. The non-Hermitian Hopf insulator thus offers a manageable model for studying non-Hermitian properties beyond the standard classification of topological systems.

The rest of the paper is organized as follows. Section II reviews the Hermitian Hopf insulator and presents a generalization to the non-Hermitian setting with a gen-

eralized expression of the Hopf index. Section III shows the quantized values of the modulus of the Hopf index and the energy spectrum of the non-Hermitian model. A bulk-boundary correspondence is established in the non-Hermitian model. Section IV concludes our work.

## II. THEORETICAL BACKGROUND

### A. Review of Hermitian Hopf insulator

Following Ref.<sup>27</sup>, we construct a 3D two-band Hermitian model with a nontrivial Hopf index  $\chi$  and zero Chern numbers  $C_{x,y,z}$  on the three sub-2D tori. By defining

$$\begin{aligned} u_1(\mathbf{k}) &= \sin k_x + i \sin k_y, \\ u_2(\mathbf{k}) &= \sin k_z + i(\cos k_x + \cos k_y + \cos k_z + h), \end{aligned}$$

the 3D two-band Hamiltonian in a dimensionless form is given by

$$H = \sum_{i=1}^3 d_i \sigma^i, \quad d_i = \sum_{a,b=1}^2 u_a^* \sigma_{ab}^i u_b. \quad (1)$$

Here  $*$  denotes the complex conjugate,  $h$  is a constant parameter, and  $\sigma_i$  with  $i = 1, 2, 3$  denotes the Pauli matrices. The Hamiltonian actually defines a map from  $T^3$  to  $S^2$ . To see this, we can normalize  $u_a$  by introducing

$$z_a = \frac{u_a}{\sqrt{|u_1|^2 + |u_2|^2}}, \quad (a = 1, 2). \quad (2)$$

This leads to  $|z_1|^2 + |z_2|^2 = 1$ , which describes a unit 3D sphere in  $\mathbb{R}^4$ . Thus,  $z_a(\mathbf{k})$  gives a map from  $T^3$  to  $S^3$ . We can also define the normalized  $d_i$  by  $R_i = \sum_{a,b=1}^2 z_a^* \sigma_{ab}^i z_b$ , or more explicitly by

$$R_1 = \text{Re}(2z_1 z_2^*), \quad R_2 = \text{Im}(2z_1 z_2^*), \quad R_3 = |z_1|^2 - |z_2|^2.$$

It follows that  $\sum_{i=1}^3 R_i^2 = 1$ , which describes a unit 2D sphere in  $\mathbb{R}^3$ . Thus,  $R_i$  gives a map from  $S^3$  to  $S^2$ . This is the Hopf map<sup>35</sup> originally introduced by H. Hopf<sup>36</sup>. The composition of the above two maps gives the desired map from  $T^3$  to  $S^2$  with a nonzero Hopf index.

We mention that in Ref.<sup>28</sup>, the model of Eq. (1) has been generalized to one with  $d_i = (u^*)^p \sigma^i u^q$ . Here  $p$  and  $q$  are integers. The generalized model gives rise to a higher Hopf index. In those generalized models, it is found that the number of edge states is usually larger than the Hopf index. For instance, Ref.<sup>28</sup> shows four surface states when the corresponding Hopf index is two. Nevertheless, we will restrict our discussion to the simplest case of Eq. (1) with an established bulk-boundary correspondence and generalize it to a non-Hermitian model.

In order to give an explicit formula for the Hopf index, we first notice that the Berry curvature for a 3D two-band model can be written as

$$F_{\mu\nu} = \frac{1}{2} \mathbf{R} \cdot (\partial_\mu \mathbf{R} \times \partial_\nu \mathbf{R}). \quad (3)$$

Here  $\mu, \nu = k_x, k_y, k_z$  and  $\partial_\mu = \frac{\partial}{\partial k_\mu}$ . In terms of the variable  $z_a$ , the Berry curvature can be written as the curl of a globally defined vector potential<sup>37</sup>, given by

$$A_\mu = \frac{i}{2} \sum_a [z_a^* (\partial_\mu z_a) - (\partial_\mu z_a^*) z_a], \quad (4)$$

$$\begin{aligned} F_{\mu\nu} &= \partial_\mu A_\nu - \partial_\nu A_\mu \\ &= -i \sum_a [(\partial_\mu z_a^*) (\partial_\nu z_a) - (\partial_\nu z_a^*) (\partial_\mu z_a)]. \end{aligned} \quad (5)$$

The Hopf index then follows the expression

$$\chi = \frac{1}{8\pi^2} \int_{BZ} \epsilon_{\mu\nu\rho} A_\mu F_{\nu\rho} d^3 k. \quad (6)$$

Here  $\epsilon_{\mu\nu\rho}$  is the Levi-Civita symbol. For the specific model studied here, we find

$$\chi = \frac{1}{2\pi^2} \int_{BZ} \frac{(s_2 + hs_3)}{(3 + h^2 + 2s_2 + 2hs_1)^2} d^3 k; \quad (7)$$

$$s_1 = \cos k_x + \cos k_y + \cos k_z,$$

$$s_2 = \cos k_x \cos k_y + \cos k_y \cos k_z + \cos k_z \cos k_x,$$

$$s_3 = \cos k_x \cos k_y \cos k_z.$$

The Hopf index then has the following values:

$$\chi = \begin{cases} -2, & |h| < 1; \\ 1, & 1 < |h| < 3; \\ 0, & |h| > 3. \end{cases} \quad (8)$$

At the transition points  $|h| = 1$  and  $|h| = 3$ , the dispersion becomes gapless and the two bands actually merge into one. The Hopf index is not well-defined at those transition points.

The Hopf index defined above can only characterize the homotopy of the mappings from  $S^3$  to  $S^2$ . The actual parameter space  $T^3$  contains non-contractible cycles, which make the topology of the mappings from  $T^3 \rightarrow S^2$  more complicated. As pointed out in Ref.<sup>27</sup>, if the system on a 2D sub-torus of  $T^3$  has a non-zero Chern number, the homotopy of the mappings from  $T^3 \rightarrow S^2$  is a finite group rather than  $\mathbb{Z}$ . This case is considered in detail in Ref.<sup>38</sup>. Here we verify that the complicated situation does not occur in the model shown in Eq. (1). With a fixed value of  $k_x$ , it can be shown that the Berry curvature satisfies  $F_x(k_y, k_z) = -F_x(-k_y, -k_z)$ . Thus, the Chern number in this direction is zero<sup>28</sup>:  $C_x = \int dk_y dk_z F_x(k_y, k_z) = 0$ . Similarly, we also have  $C_y = 0 = C_z$ . Therefore, the Hopf index of the model (1) takes values in  $\mathbb{Z}$  instead of a finite group.

### B. Non-Hermitian Hopf insulator

Now we generalize the Hopf insulator to a non-Hermitian one with the Hamiltonian

$$H = d_1 \sigma^1 + d_2 \sigma^2 + (d_3 + i\gamma) \sigma_3; \quad (9)$$

$$d_1 = \text{Re}(2u_1 u_2^*), \quad d_2 = \text{Im}(2u_1 u_2^*), \quad d_3 = |u_1|^2 - |u_2|^2.$$

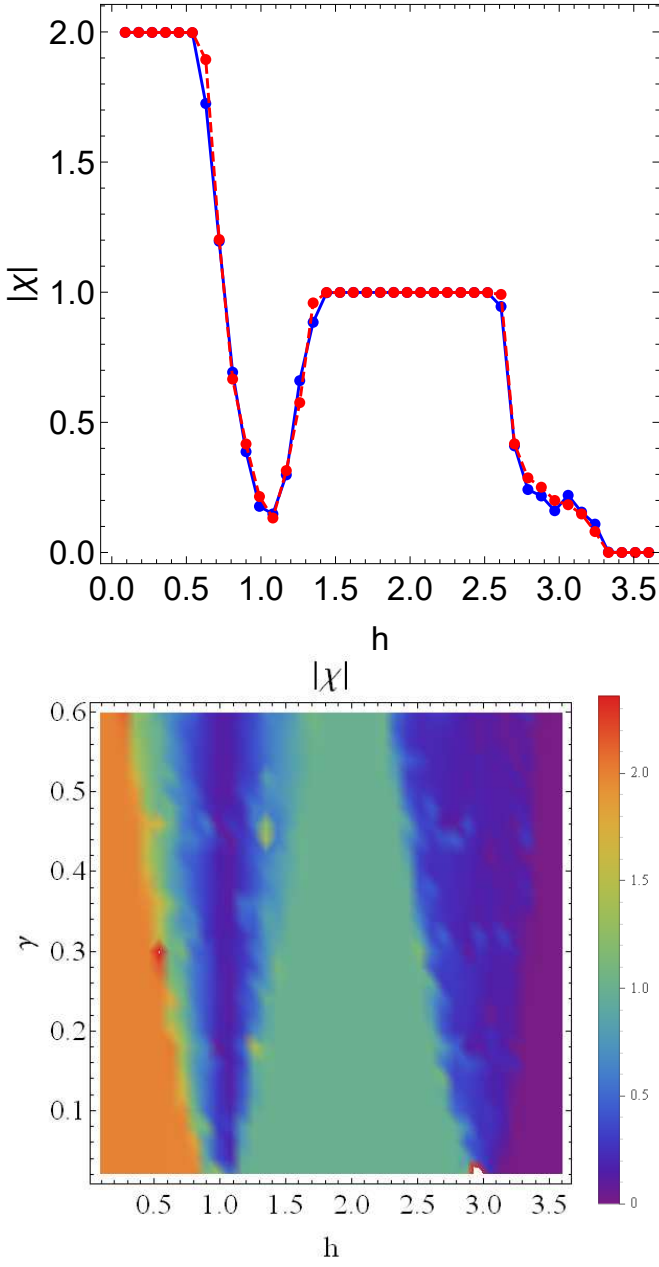


Figure 1. (Top) The modulus of the Hopf index,  $|\chi|$ , as a function of  $h$  with  $\gamma = 0.2$ . The blue solid line and the red dashed line correspond to the grid size  $N = 64$  and  $N = 128$ , respectively. (Bottom)  $|\chi|$  as a function of  $h$  and  $\gamma$ . The grid size along one direction is  $N = 64$ .

Here  $h$  and  $\gamma$  are real-valued parameters. The two eigenvalues of this Hamiltonian are

$$E_{1,2} = \pm \sqrt{d_1^2 + d_2^2 + (d_3 + i\gamma)^2}. \quad (10)$$

Because of the appearance of the imaginary part, the above spectrum is generally complex-valued.

Similar to the Hermitian case, we define the following

normalized vector with the components

$$R_1 = \frac{d_1}{d_0}, \quad R_2 = \frac{d_2}{d_0}, \quad R_3 = \frac{d_3 + i\gamma}{d_0}. \quad (11)$$

Here  $d_0 = \sqrt{d_1^2 + d_2^2 + (d_3 + i\gamma)^2}$ . Note that the normalization factor  $d_0$  is also a complex number in the non-Hermitian model. Although it may look natural to define the normalization factor as the norm of the vector  $\mathbf{d}$ , we instead choose  $d_0$  to define the normalized vector  $\mathbf{R}$  in order to maintain the same eigenstate projectors  $P_{1,2}$  as those of the Hermitian case. Explicitly,

$$P_{1,2} = \frac{1}{2} \left( 1 \pm \sum_i R_i \sigma_i \right). \quad (12)$$

The Berry curvature can be expressed in terms of the projectors as

$$F_{\mu\nu} = i \text{Tr} \left( P_1 [\partial_\mu P_1, \partial_\nu P_1] \right). \quad (13)$$

In the non-Hermitian model, therefore,  $F_{\mu\nu}$  is still given by the expression shown in Eq. (3). We remark that in the non-Hermitian model, the components of  $\mathbf{R}$  are complex numbers. Thus, the Berry curvature is also complex. It is convenient to express the Berry curvature as a 3-component dual vector

$$B_\rho(\mathbf{k}) = \frac{1}{2} \epsilon_{\rho\mu\nu} F_{\mu\nu}. \quad (14)$$

Here the indices  $\rho, \mu, \nu$  take values of  $k_x, k_y$ , and  $k_z$ .

For the non-Hermitian case, it is challenging to find an explicit, analytical expression of the Berry connection  $A_\mu$  similar to the one shown in Eq. (4) for the Hermitian case. Nevertheless, we compute the Hopf index numerically. In order to solve the curl equation  $\nabla \times \mathbf{A} = \mathbf{B}$ , we take a Fourier transform of the Berry curvature as follows.

$$B_\mu(\mathbf{r}) = \frac{1}{N^{3/2}} \sum_{\mathbf{k}} B_\mu(\mathbf{k}) e^{i\mathbf{k} \cdot \mathbf{r}}. \quad (15)$$

Here  $k_{x,y,z}$  take values from  $\{-\pi, -\pi + \frac{2\pi}{N}, \dots, \pi - \frac{2\pi}{N}\}$ , and  $N$  is the number of lattice sites along one direction. Similarly,  $r_{x,y,z}$  takes values from  $\{-\frac{N}{2}, -\frac{N}{2} + 1, \dots, \frac{N}{2} - 1\}$ . The curl equation then becomes  $(-i\mathbf{r}) \times \mathbf{A} = \mathbf{B}$ . Under the gauge choice  $\nabla \cdot \mathbf{A} = 0$ , the Berry connection can be found as

$$\mathbf{A}(\mathbf{r}) = -i \frac{\mathbf{r} \times \mathbf{B}(\mathbf{r})}{r^2}. \quad (16)$$

Although the Hopf index depends on the Berry connection, it is known that the Abelian Chern-Simons term is gauge invariant up to a surface term<sup>26</sup>. Afterwards, the Hopf index of the non-Hermitian case is given by

$$\chi = -\frac{(2\pi)^3}{N^3(4\pi^2)} \sum_{\mathbf{r}} \mathbf{B}(-\mathbf{r}) \cdot \mathbf{A}(\mathbf{r}). \quad (17)$$

In general, the generalized Hopf index is complex-valued.

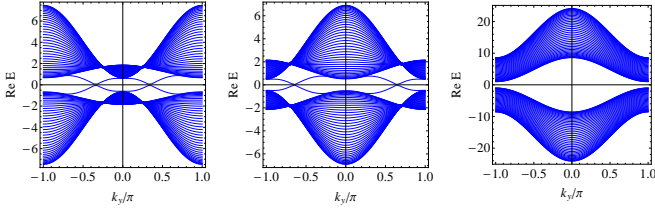


Figure 2. Energy spectrum of the non-Hermitian Hopf model as a function of  $k_y$  with open boundary along the  $z$  direction. We take  $k_x = 2.7$  as an example. The left, middle, and right panels correspond to  $h = 0.2, 1.5, 3.8$ , respectively.

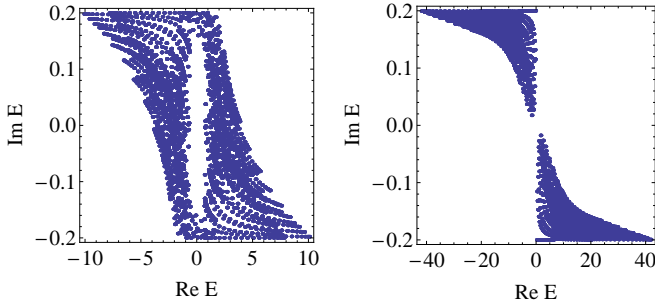


Figure 3. Energy spectrum of the non-Hermitian Hopf model on the complex plane, showing the edge states connecting the two bands (left) and no edge state (right). The left (right) panel shows the case with  $h = 0.2$  and  $\gamma = 0.2$  ( $h = 3.5$  and  $\gamma = 0.2$ ). The system has open boundary condition along the  $z$ -direction and periodic boundary condition along the other two directions.

### III. RESULTS AND DISCUSSIONS

Here we present the numerical results of the Hopf index of the non-Hermitian model with periodic boundary condition. In computing the Hopf index, we have compared the results from  $N = 64$  and  $N = 128$  grid-points. As shown in the top panel of Figure 1, the two sets of data are virtually on top of each other. Thus, the grid size of  $N = 64$  is large enough to give stable results, and in the following we present the data with  $N = 64$  unless specified otherwise.

The top panel of Figure 1 shows the modulus of the Hopf index,  $|\chi|$ , as a function of  $h$  for  $\gamma = 0.2$ . One can see that  $|\chi| = 2$  within  $0 < h < 0.5$  and  $|\chi| = 1$  within  $1.5 < h < 2.5$ . When  $h > 3$ , the Hopf index gradually approaches zero,  $|\chi| = 0$ . This is very similar to the case of the Hermitian Hopf insulator. However, one important difference is that the Hopf index of the non-Hermitian model is not strictly quantized around the transition points at  $h = 1$  and  $h = 3$ . Instead, the Hopf index quickly drops to almost zero around those transition points. The reason is that within  $0.6 < h < 1.4$  and  $2.5 < h < 3.2$ , the dispersion becomes gapless for the non-Hermitian model. Therefore, the Hopf index ob-

tained numerically approaches zero. In the bottom panel of Figure 1, we plot  $|\chi|$  as a function of both  $h$  and  $\gamma$ , showing where  $|\chi| = 2, 1, 0$ , can be found in the parameter space, respectively. The two dark blue areas around  $h = 1$  and  $h = 3$  are the gapless transition regions. As  $\gamma$  increases, the gapless regions increases as well.

The ranges of the gapless regions can be determined as follows. In momentum space, the two energy bands are given by  $E = \pm\sqrt{d_1^2 + d_2^2 + (d_3 + i\gamma)^2}$ . The condition for the two bands to close at  $E = 0$  can be expressed as

$$d_1^2 + d_2^2 + d_3^2 - \gamma^2 = 0, \quad d_3 = 0. \quad (18)$$

This is equivalent to the following condition

$$|u_1|^2 = \frac{\gamma}{2}, \quad |u_2|^2 = \frac{\gamma}{2}. \quad (19)$$

For a given  $\gamma$ , the above two equations have real-valued solutions  $\mathbf{k}$  for certain ranges of the parameter  $h$ , which in turn determine the size of the gapless regions. It can be numerically verified that at the boundaries of the gapless regions, one always has  $k_z = 0$  and  $k_y = \pi$  or  $k_z = \pi$  and  $k_y = \pi$ . Hence, it can be shown that the gapless regions are given by

$$\sqrt{1 - \frac{\gamma}{2}} - \sqrt{\frac{\gamma}{2}} < h < \sqrt{1 - \frac{\gamma}{2}} + \sqrt{\frac{\gamma}{2}}, \quad (20)$$

$$2 + \sqrt{1 - \frac{\gamma}{2}} - \sqrt{\frac{\gamma}{2}} < h < 2 + \sqrt{1 - \frac{\gamma}{2}} + \sqrt{\frac{\gamma}{2}}. \quad (21)$$

After analyzing the Hopf index of the non-Hermitian Hopf insulator with periodic boundary condition, we investigate its edge states when open boundary is present. In the following, we will consider the model with open boundary condition along the  $z$  direction while maintaining periodic boundary condition along the  $x, y$  directions. The Hamiltonian is then given by

$$\begin{aligned} H' = & \left[ (\sin k_y - i \sin k_x) \sigma_1 \right. \\ & + (\sin k_x + i \sin k_y) \sigma_2 - h_k \sigma_3 \left. \right] \otimes h_0 + \text{H.c.} \\ & + \left[ 2h_k \sin k_y \sigma_1 + 2h_k \sin k_x \sigma_2 \right. \\ & \left. + (\sin^2 k_x + \sin^2 k_y - h_k^2 - 1 + i\gamma) \sigma_3 \right] \otimes I_0. \end{aligned} \quad (22)$$

Here we define  $h_k = h + \cos k_x + \cos k_y$ , and  $h_0 = \delta_{i+1,j}$  and  $I_0 = \delta_{ij}$  are  $N_z \times N_z$  matrices with  $i, j = 1, \dots, N_z$ . In Figure 2, we show the energy spectrum of  $H'$  as a function of  $k_y$  with fixed  $k_x = 2.7$ . From left to right, we choose  $h = 0.2, 1.5, 3.8$ , respectively. One can see there are two zero-energy crossings in the left and middle panels, but there is no zero-energy crossing in the right panel. The crossings signify the edge states at the open boundary, which will be analyzed after the presentation of the energy spectrum.

Figure 3 shows two typical examples of the energy eigenvalues of Eq. (22) on the complex plane. Here we take  $N_z = 20$  points along the  $z$ -direction, and 26 points along the  $k_x$  and  $k_y$  directions, respectively, with  $\gamma = 0.2$ .

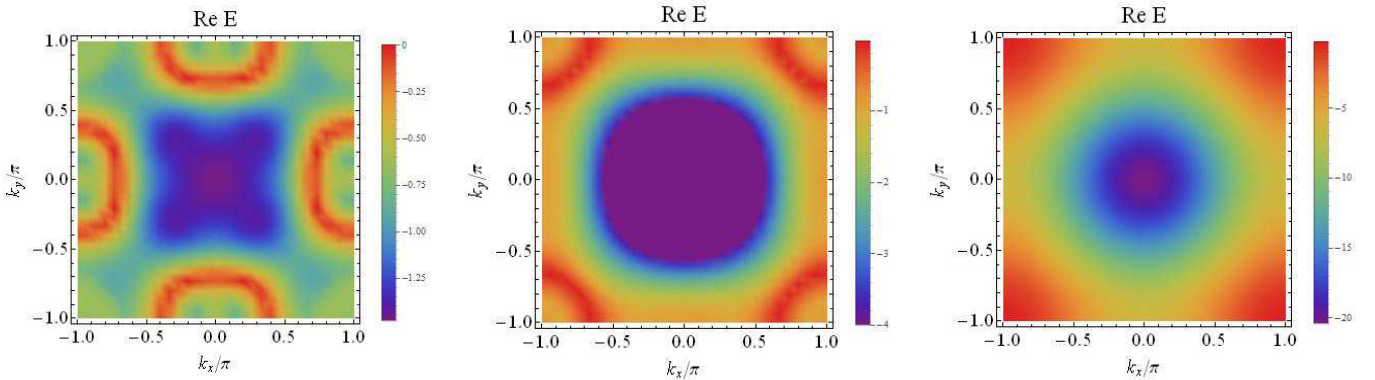


Figure 4. Energy spectrum of the eigenstate closest to the zero energy as a function of  $k_x$  and  $k_y$  with open boundary along the  $z$  direction. From left to right,  $h = 0.2, 1.9, 3.5$ , showing 2, 1, and 0 zero-energy Fermi rings, respectively. We take  $\gamma = 0.2$ .

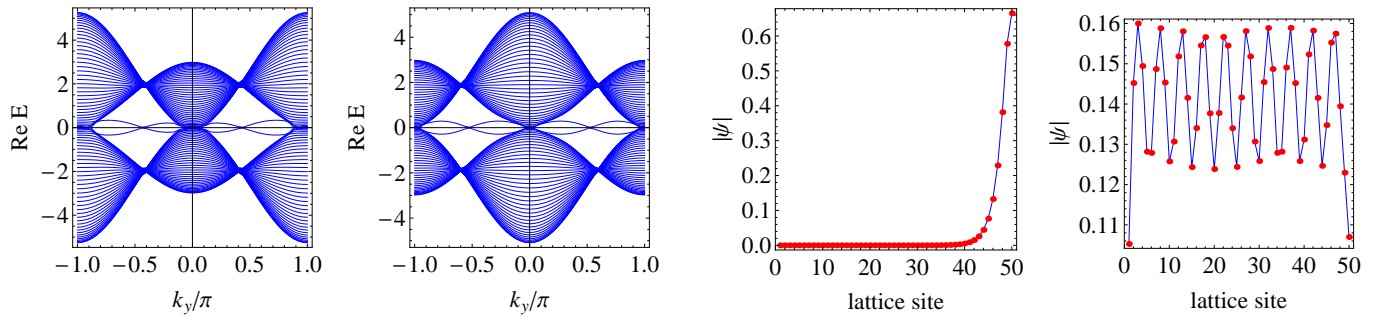


Figure 5. Energy spectrum of the non-Hermitian Hopf model as a function of  $k_y$  with open boundary along the  $z$  direction and  $\gamma = 0.2$ . For the left (right) panel,  $h = 0.67$  and  $k_x = 2.84$  ( $h = 1.26$  and  $k_x = 3.04$ ). The gap closes in both cases.

The two examples are from  $h = 0.2$  and  $h = 3.5$ , shown on the left and right panels, respectively. On the left panel, there are two separate clusters of eigenvalues corresponding to the two bands. There are also some edge states connecting those two bands, forming an enclosed, hollow region on the complex plane. On the right panel, in contrast, there are only two separate clusters of points, corresponding to the two bands. We found that if  $|\chi| > 0$  and the system is gapped, the energy spectrum is qualitatively similar to the left panel of Figure 3. In contrast, if the system is gapped with  $\chi = 0$ , the spectrum is qualitatively similar to the right panel. However, the plots of the energy spectrum on the complex plane cannot unambiguously disclose the relation with the Hopf index.

For a deeper understanding of the edge states crossing the energy gap, we analyze the energy spectrum as a function of  $k_x$  and  $k_y$ . For each eigenstate, the corresponding eigen-energy forms a curved surface above the  $k_x$  and  $k_y$  plane. To avoid a messy view of a lot of overlapped eigen-energy surfaces, we choose to plot only the

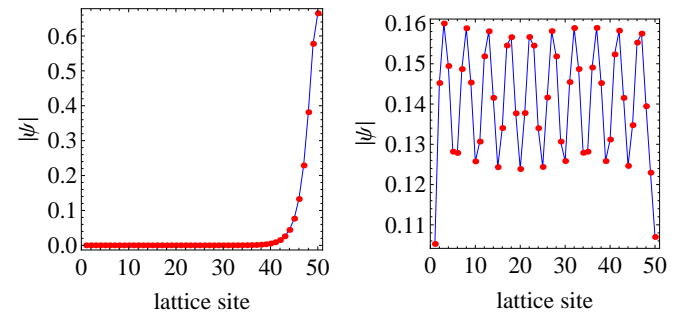


Figure 6. The amplitude  $|\psi|$  of the wavefunctions of an edge state (left panel) and a selected bulk state (right panel). Here  $h = 0.5$ ,  $k_x = 0.2$ , and  $k_y = 2.3$ .

eigen-energy surface that is closest to the zero-energy and show it in Figure 4. Here we only present the part of the eigen-energy surface below the zero-energy because the part above the zero-energy has a very similar shape. We choose  $h = 0.2, 1.9, 3.5$  to represent the system with distinct values of the Hopf index. One can see that there is a ring structure with zero-energy around  $\mathbf{k} = (\pm\pi, \pm\pi)$  when  $h = 1.9$ . Such a structure is known as the Fermi ring<sup>29</sup>. On the other hand, there are two Fermi rings around  $\mathbf{k} = (\pm\pi, 0)$  and  $(0, \pm\pi)$  when  $h = 0.2$ . In contrast, there is no Fermi ring when  $h = 3.5$ . The corresponding values of the modulus of the hopf index are 2, 1, and 0, respectively. We have verified that in the gapped regimes, the number of the Fermi rings is the same as the corresponding value of the modulus of the Hopf index, thereby established a bulk-boundary correspondence for the non-Hermitian model.

The qualitative feature of the Fermi ring is the same for both Hermitian and non-Hermitian Hopf insulators. The unique property of the non-Hermitian model is a finite region of  $h$  that the energy spectrum is gapless for a fixed

$\gamma$ . In contrast, the Hermitian model is gapless only at isolated points of  $h$ . The size of the gapless regions have been determined by Eqs. (20) and (21) in the calculation with periodic boundary condition. Interestingly, we can also determine the boundaries of the gapless regions of the same system with open boundary condition along the  $z$  direction. In Figure 5, we show the energy spectrum of the non-Hermitian model with open boundary condition along the  $z$ -axis and  $\gamma = 0.2$  as a function of  $k_y$  for  $h = 0.67$  (left panel) and  $h = 1.26$  (right panel). One can clearly see that the two bulk bands close at those values of  $h$ . By analyzing the energy spectrum, we found that the gap remains closed when  $0.67 < h < 1.26$ . The other gapless region can be found within  $2.6 < h < 3.3$ .

Importantly, the ranges of the gapless regimes determined by the open-boundary results are numerically identical to the values given by Eqs. (20) and (21). Thus, the gapless regimes of the non-Hermitian Hopf insulator estimated from open- and periodic-boundary cases agree. It is known that in some exemplary 1D and 2D non-Hermitian models, the spectrum with open boundary condition may be quite different from that with periodic boundary condition<sup>33,34</sup>. The agreement of the spectra of the non-Hermitian Hopf model with different boundary conditions may be because it is a 3D model and we impose open boundary condition only along one direction while the other two directions have periodic boundary condition. Nevertheless, the non-Hermitian Hopf model offers an example showing a robust spectrum against a change of the boundary condition. We remark that within the gapless regions, the concept of the edge states may no longer be meaningful.

To confirm the states that cross the zero-energy are localized at the open boundary in the gapped regions, Fig. 6 shows the amplitudes of the wavefunctions of an edge state and a selected bulk state of a chosen set of parameters. We have used a larger system size ( $N = 50$ ) to contrast the difference between the edge and bulk states. As shown in the left panel of Fig. 6, the localization of the edge states is visible in the non-Hermitian Hopf model. In order to have a qualitative understanding of the edge

state wavefunction, we consider the Hermitian Hopf insulator and approximate it by a continuum model. At the Fermi ring, we have  $d_3 \approx 0$ . Then, the Hamiltonian may be approximated by  $H = d_1\sigma_1 + d_2\sigma_2$ . The real part of the corresponding zero-energy eigen-equation is given by

$$(A + \frac{\partial}{\partial z})\psi = 0 \quad (23)$$

with  $A = (1 + h + \cos k_x + \cos k_y)$ . From the approximation, we find the edge-state wavefunction to be  $\psi \sim \exp(-A z)$ , which shows an exponential decay away from the open boundary. Our numerical results suggest the edge states of the non-Hermitian model exhibits similar localization behavior.

#### IV. CONCLUSION

A non-Hermitian generalization of the 3D two-band Hopf insulator has been analyzed. The Hopf index has been generalized to the non-Hermitian model, and its modulus exhibits quantized values in the gapped regimes. From the energy spectrum of the non-Hermitian model with open boundary condition, we found a bulk-boundary correspondence between the modulus of the Hopf index and the number of zero-energy Fermi rings. The isolated gapless points of the Hermitian Hopf model are broadened into finite regimes with a gapless spectrum. Importantly, the gapless regimes estimated from the periodic- and open- boundary cases agree with each other. Moreover, the edge states in the gapped regimes are shown to localized at the open boundary. The analysis of the Hopf insulator offers an alternative view of topological systems and advance our understanding of their non-Hermitian generalizations.

#### ACKNOWLEDGMENTS

Y. H was supported by the National Natural Science Foundation of China under Grant No. 11874272.

\* heyan\_ctp@scu.edu.cn

† cchien5@ucmerced.edu

<sup>1</sup> M. Z. Hasan and C. L. Kane, Rev. Mod. Phys. **82**, 3045 (2010).

<sup>2</sup> X.-L. Qi and S.-C. Zhang, Rev. Mod. Phys. **83**, 1057 (2011).

<sup>3</sup> C.-K. Chiu, J. C. Y. Teo, A. P. Schnyder, and S. Ryu, Rev. Mod. Phys. **88**, 035005 (2016).

<sup>4</sup> T. E. Lee, Phys. Rev. Lett. **116**, 133903 (2016).

<sup>5</sup> D. Leykam, K. Y. Bliokh, C. Huang, Y. D. Chong, and F. Nori, Phys. Rev. Lett. **118**, 040401 (2017).

<sup>6</sup> S. Yao and Z. Wang, Phys. Rev. Lett. **121**, 086803 (2018).

<sup>7</sup> H. Shen, B. Zhen, and L. Fu, Phys. Rev. Lett. **120**, 146402 (2018).

<sup>8</sup> Z. Gong, Y. Ashida, K. Kawabata, K. Takasan, S. Higashikawa, and M. Ueda, Phys. Rev. X **8**, 031079 (2018).

<sup>9</sup> K. Kawabata, S. Higashikawa, Z. Gong, Y. Ashida, and M. Ueda, Nat. Comm. **10**, 297 (2019).

<sup>10</sup> F. K. Kunst, E. Edvardsson, J. C. Budich, and E. J. Bergholtz, Phys. Rev. Lett. **121**, 026808 (2018).

<sup>11</sup> K. I. Imura and Y. Takane (2019), arXiv: 1908.09438.

<sup>12</sup> R. Koch and J. C. Budich, *Bulk-boundary correspondence in non-hermitian systems: Stability analysis for generalized boundary conditions* (2019), arXiv: 1912.07687.

<sup>13</sup> K. Yokomizo and S. Murakami, Phys. Rev. Lett. **123**, 066404 (2019).

<sup>14</sup> E. Lee, H. Lee, and B. J. Yang, *Many-body approach to non-hermitian physics in fermionic systems* (2019), arXiv:

1912.05825.

<sup>15</sup> F. Song, S. Yao, and Z. Wang, Phys. Rev. Lett. **123**, 170401 (2019).

<sup>16</sup> C. Yuce, Phys. Rev. A **99**, 032109 (2019).

<sup>17</sup> Z. Li and R. S. K. Mong, *Homotopical classification of non-hermitian band structures* (2019), arXiv: 1911.02697.

<sup>18</sup> C. C. Wojcik, X. Q. Sun, T. Bzdusek, and S. Fan, *Topological classification of non-hermitian hamiltonians* (2019), arXiv: 1911.12748.

<sup>19</sup> W. X, Z. H. Zhang, Z. C. Gu, and W. Q. Chen, *Classification of topological phases in one dimensional interacting non-hermitian systems and emergent unitarity* (2019), arXiv: 1911.01590.

<sup>20</sup> T. Bessho, K. Kawabata, and M. Sato, *Topological classification of non-hermitian gapless phases: Exceptional points and bulk fermi arcs* (2019), arXiv: 1911.08998.

<sup>21</sup> H. Zhou and J. Y. Lee, Phys. Rev. B **99**, 235112 (2019).

<sup>22</sup> R. El-Ganainy, K. G. Makris, M. Khajavikhan, Z. H. Musslimani, S. Rotter, and D. N. Christodoulides, Nat. Phys. **14**, 11 (2018).

<sup>23</sup> W. Zhu, X. Fang, D. Li, Y. Sun, Y. Li, Y. Jing, and H. Chen, Phys. Rev. Lett. **121**, 124501 (2018).

<sup>24</sup> C. Scheibner, W. T. M. Irvine, and V. Vitelli, *Non-hermitian band topology in active and dissipative mechanical metamaterials* (2020), arXiv: 2001.04969.

<sup>25</sup> W. Gou, T. Chen, D. Xie, T. Xiao, T. S. Deng, B. Gadway, W. Yi, and B. Yan, *Tunable non-reciprocal quantum transport through a dissipative aharonov-bohm ring in ultracold atoms* (2020), arXiv: 2001.01859.

<sup>26</sup> M. Nakahara, *Geometry, Topology and Physics, second edition* (Taylor and Francis Group, New York, 2003).

<sup>27</sup> J. E. Moore, Y. Ran, and X.-G. Wen, Phys. Rev. Lett. **101**, 186805 (2008).

<sup>28</sup> D. L. Deng, S. T. Wang, C. Shen, and L. M. Duan, Phys. Rev. B **88**, 201105(R) (2013).

<sup>29</sup> C. Liu, F. Vafa, and C. Xu, Phys. Rev. B **95**, 161116(R) (2017).

<sup>30</sup> X. X. Yuan, L. He, S. T. Wang, D. L. Deng, F. Wang, W. Q. Lian, X. Wang, C. H. Zhang, H. L. Zhang, X. Y. Chang, et al., Chin. Phys. Lett. **34**, 060302 (2017).

<sup>31</sup> C. R. Yi, J. L. Yu, W. Sun, X. T. Xu, S. Chen, and J. W. Pan, *Observation of the hopf links and hopf fibration in a 2d topological raman lattice* (2019), arXiv: 1904.11656.

<sup>32</sup> T. Schuster, F. Flicker, M. Li, S. Kotochigova, J. E. Moore, J. Ye, and N. Y. Yao, *Realizing hopf insulators in dipolar spin systems* (2019), arXiv:1901.08597.

<sup>33</sup> S. Yao and Z. Wang, Phys. Rev. Lett. **121**, 086803 (2018).

<sup>34</sup> S. Yao, F. Song, and Z. Wang, Phys. Rev. Lett. **121**, 136802 (2018).

<sup>35</sup> J. H. C. Whitehead, Proc. Natl. Acad. Sci. **33**, 117 (1947).

<sup>36</sup> H. Hopf, Math. Ann. **104**, 637 (1931).

<sup>37</sup> E. Fradkin, *Field Theories of Condensed Matter Physics* (Cambridge University Press, Cambridge, UK, 2013), 2nd ed.

<sup>38</sup> R. Kennedy, Phys. Rev. B **94**, 035137 (2016).